USING THE ORTHOGONAL PROJECTION FOR PARAMETER INITIALIZATION IN THE 3D RECONSTRUCTION OF DISTANT OBJECTS

Keith F. Blonquist, Junior Project Engineer
Lidar Pacific Corporation
Logan, UT 84341
kfblonquist@lidarpacific.com

Robert T. Pack, Associate Professor
Utah State University
Logan, UT 84322
robert.pack@usu.edu

ABSTRACT

We present a method for the 3D reconstruction of objects from images captured in a surveillance setting using un-calibrated hand-held cameras. The images considered are of distant objects occupying a small portion of the field-of-view (FOV); have been captured in a non-systematic manner from varying aspects, distances, and angles; and have no *a priori* target information for 3D coordinates or scale. The current algorithms used to estimate camera orientations and perform 3D reconstruction rely to some degree on initial approximations of camera orientation and/or 3D coordinates of the target object or control points. Parameter initialization in most surveillance applications is problematic due to the non-regular camera arrangements and lack of target information. Using some of the strengths of the orthogonal model, this paper presents a robust initial approximation method suited to the demands of surveillance imagery. The method assumes initially that the images are orthogonal, allowing for a direct linear solution without the necessity of initial approximations. The accuracy of the approximations from the orthogonal method can then be improved using a "perspective-corrected" orthogonal projection that incorporates the approximate data in order to adjust the images from perspective images to nearly orthogonal images. Finally, the "perspective-corrected" orthogonal solution is used to approximate the camera orientations, and a standard bundle adjustment based on the perspective projection can be carried out. The reliability of the method using varying imaging distances and cameras is demonstrated through experimentation with images taken in the field.

INTRODUCTION

Images of distant objects captured in a surveillance setting are quite often taken with uncalibrated, hand-held cameras, using long lenses. Also, these images are often taken from un-systematic, random aspects and from widely varying distances. Thus the target generally only fills a small portion of the field-of-view (FOV) of each image, and there is generally no control information for the target or for the locations from which the images were taken relative to the target. Hence, the only *a priori* information available from a set of surveillance images is 1) a set of point correspondences across the images, and 2) the approximate interior orientation parameters (IOP) of the cameras used. All of these factors combine to make the 3D reconstruction of targets from surveillance imagery a difficult task. Specifically, it is a challenge to obtain initial approximations of the image orientations and target coordinates required to perform a bundle adjustment.

Bundle adjustment is the fundamental algorithm used for determining target geometry and image orientations. It is an iterative procedure that requires initial approximations. Usually, these initial approximations are obtained through the relative orientation of image pairs and subsequent intersection of the points that appear on both images. Then, the approximate orientations of additional images can be obtained using the Direct Linear Transformation (DLT).

However, due to the narrow FOV that is common in surveillance imagery, the above methods (relative orientation and DLT) can be unreliable and unstable. It is well known that algorithms based on perspective geometry are subject to poor performance in situations where the FOV is narrow. Thus, for many surveillance image sets, initial approximations have to be obtained in another manner.

The orthogonal projection has been shown to be a reliable alternative to the perspective projection in long-range narrow FOV applications. However, much of the research that has been conducted for the orthogonal

projection is related to satellite imagery, rather than non-topographic imagery. Hence, in much of the literature, assumptions have been made that do not necessarily hold true when considering the irregular image configurations encountered in surveillance imagery.

Thus, we develop a comprehensive algorithm for the 3D reconstruction of distant objects utilizing both the orthogonal and perspective projections. By assuming initially that the images are orthogonal, we derive initial approximations from a set of point correspondences alone using an algorithm based on orthogonal geometry. Using these approximations, bundle adjustment based on the orthogonal projection can be performed to refine the initial approximation. Next, a perspective-correction is performed on the original image coordinates, which transforms them from perspective images to nearly orthogonal images. These perspective-corrected image coordinates are then fed into the orthogonal bundle adjustment, resulting in an improved intermediate solution. Finally, the perspective-corrected solution is used as an initial approximation for the standard perspective bundle adjustment.

The resulting algorithm has the stability and robustness of the orthogonal projection, which is necessary to evaluate narrow FOV images. Yet, it also has the accuracy of the perspective projection, which is a more exact model of the images. The algorithm's performance is demonstrated with several image sets, both real and synthetic.

THEORY

The orthogonal projection as defined herein is a six-parameter projection involving three degrees of freedom for rotation, one degree of freedom for scale, and two degrees of freedom for a shift in the image space. These six degrees of freedom account for both the interior and exterior orientation of the image. The projection equations are given by

$$\begin{aligned} x &= T_{11}X + T_{12}Y + T_{13}Z + \Delta x \\ y &= T_{21}X + T_{22}Y + T_{23}Z + \Delta y \end{aligned} \qquad (1)$$

where (x, y) are the image coordinates of a point on the target, (X, Y, Z) are the object-space coordinates of the point, T_{ij} are terms from the scaled rotation matrix **T**, and $(\Delta x, \Delta y)$ are shift terms in image space. The scaled rotation matrix **T** can be expressed by

$$\mathbf{T} = \begin{bmatrix} qw^2 + qx^2 - qy^2 - qz^2 & 2(qxqy - qzqw) & 2(qxqz + qyqw) \\ 2(qxqy + qzqw) & qw^2 - qx^2 + qy^2 - qz^2 & 2(qyqz - qxqw) \\ 2(qxqz - qyqw) & 2(qyqz + qxqw) & qw^2 - qx^2 - qy^2 + qz^2 \end{bmatrix} \qquad (2)$$

where (qx, qy, qz, qw) is an un-normalized quaternion. Hence, the matrix $\mathbf{T}$ has four degrees of freedom (for rotation and scale) and the shift terms $(\Delta x, \Delta y)$ account for the other two degrees of freedom, for a total of six.

On the other hand, the perspective projection is given by the well-known collinearity equations

$$\begin{aligned} x &= xa - f\frac{r_{11}(X - Xc) + r_{12}(Y - Yc) + r_{13}(Z - Zc)}{r_{31}(X - Xc) + r_{32}(Y - Yc) + r_{33}(Z - Zc)} \\ y &= ya - f\frac{r_{21}(X - Xc) + r_{22}(Y - Yc) + r_{23}(Z - Zc)}{r_{31}(X - Xc) + r_{32}(Y - Yc) + r_{33}(Z - Zc)} \end{aligned} \qquad (3)$$

where (x, y) are the image coordinates of a point on the target, (X, Y, Z) are the object-space coordinates of the point, the r_{ij} terms are from the rotation matrix $\mathbf{R}$, (Xc, Yc, Zc) is the perspective center of the image, f is the principal distance of the camera, and (xa, ya) are the coordinates of the principal point. Note that the perspective projection has nine degrees of freedom: three for exterior rotation (imbedded in $\mathbf{R}$), three for exterior shift (Xc, Yc, Zc), and three for interior orientation (f, xa, ya).

When the imaging distance is large in comparison to the size of the object being imaged, the perspective projection can be approximated by the orthogonal projection. This is apparent when considering two alternative forms of the above equations. The orthogonal projection equation (1) can be rewritten as a matrix expression

$$\begin{bmatrix} x - \Delta x \\ y - \Delta y \\ z \end{bmatrix} = \mathbf{T}\mathbf{X} = s\mathbf{R}\mathbf{X} \tag{4}$$

where z is a z-coordinate in image space that can be ignored, $\mathbf{X} = [X \quad Y \quad Z]^T$ are the target coordinates in vector form, s is a positive scale, and $\mathbf{R}$ is a rotation matrix. The above equation (4) breaks down the scaled rotation matrix $\mathbf{T}$ into its scale s and rotation $\mathbf{R}$. The perspective projection equation (3) can also be rewritten in matrix form as

$$\begin{bmatrix} x - x_p \\ y - y_p \\ -f \end{bmatrix} = \lambda(\mathbf{X})\mathbf{R}\Delta\mathbf{X} \tag{5}$$

where $\Delta\mathbf{X} = [X - X_c \quad Y - Y_c \quad Z - Z_c]^T$ is the vector from the perspective center to the target point and $\lambda(\mathbf{X}) = -\dfrac{f}{r_{31}(X - X_c) + r_{32}(Y - Y_c) + r_{33}(Z - Z_c)}$ is the scale factor for each point. When the imaging distance is large in comparison to the size of the target, the perspective projection scales $\lambda(\mathbf{X})$ for each point are nearly equivalent. Thus, the perspective projection can be approximated by

$$\begin{bmatrix} x - x_p \\ y - y_p \\ -f \end{bmatrix} = \lambda(\mathbf{X})\mathbf{R}\Delta\mathbf{X} \approx \bar{s}\mathbf{R}\Delta\mathbf{X} \tag{6}$$

where $\bar{s}$ is the average of the individual point scales. The top two rows of the above equation (6) can then be written in the same form as the orthogonal projection as

$$\begin{aligned} x &\approx \bar{T}_{11}X + \bar{T}_{12}Y + \bar{T}_{13}Z + \Delta\bar{x} \\ y &\approx \bar{T}_{21}X + \bar{T}_{22}Y + \bar{T}_{23}Z + \Delta\bar{y} \end{aligned} \tag{7}$$

where

$$\begin{aligned} \bar{T}_{11} &= \bar{s}r_{11} \quad \bar{T}_{12} = \bar{s}r_{12} \quad \bar{T}_{13} = \bar{s}r_{13} \\ \Delta\bar{x} &= -\bar{s}(r_{11}X_c + r_{12}Y_c + r_{13}Z_c) + x_p \\ \bar{T}_{21} &= \bar{s}r_{21} \quad \bar{T}_{22} = \bar{s}r_{22} \quad \bar{T}_{23} = \bar{s}r_{23} \\ \Delta\bar{y} &= -\bar{s}(r_{21}X_c + r_{22}Y_c + r_{23}Z_c) + y_p \end{aligned} \tag{8}$$

Equations 1 and 7 demonstrate that the two projections are similar when the imaging distance is large compared to the size of the target.

To further relate the orthogonal projection and the perspective projection, Ono and Hattori (2002) derived a model wherein image coordinates are corrected for perspective, and then analyzed using the orthogonal projection equations. Similar to their method, the image coordinates can be corrected for perspective using the following equation

$$\begin{bmatrix} x_p \\ y_p \end{bmatrix} = \frac{\bar{s}}{\lambda(\mathbf{X})}\begin{bmatrix} x - x_p \\ y - y_p \end{bmatrix} + \begin{bmatrix} x_p \\ y_p \end{bmatrix} \tag{9}$$

where (x_p, y_p) are the perspective-corrected coordinates, $\bar{s}$ is the average of the individual point scales, $\lambda(\mathbf{X})$ is the scale factor for the given point, (x, y) are the original image coordinates, and (x_p, y_p) are the coordinates of the principal point. Also, given an orthogonal solution, the approximate perspective center for the corresponding perspective solution can be found with the following equation

$$\begin{bmatrix} \bar{X}_C \\ \bar{Y}_C \\ \bar{Z}_C \end{bmatrix} = \frac{1}{s} R^T \begin{bmatrix} x_a - \Delta x \\ y_a - \Delta y \\ f \end{bmatrix} \tag{10}$$

where $(\bar{X}_C, \bar{Y}_C, \bar{Z}_C)$ is the approximate perspective center, $(s, R, \Delta x, \Delta y)$ are from the orthogonal solution, and (f, x_a, y_a) are the IOP of the image.

Following is an implementation of these models to achieve a perspective bundle solution using a robust 6-step initialization procedure. Space does not allow a full theoretical development. Details can be found in a more comprehensive paper by Blonquist and Pack (2009b).

OUTLINE OF ALGORITHM

For the comprehensive algorithm, it is assumed that the only *a priori* data available from the surveillance images are 1) a set of point correspondences across at least three images, and 2) the approximate IOP of the camera(s) used to take the images. The flow chart in Figure 1 will assist in the explanation that follows.

Step 1: Orthogonal Initial Approximation Algorithm. The first step in the algorithm is to approximate the image orientations and target coordinates from the point correspondences. This is done through an algorithm based on (Huang and Lee, 1989), which utilizes the orthogonal projection equations (1). It requires that there are at least three images such that when considering any image pair, there are at least four common points on that image pair. Also, it is necessary that at least one point is visible on all of the images. The points that are common to all of the images are used to approximate the relative shifts of the images. Each image pair is then considered, and a set of coefficients is derived from that image pair based on the point correspondences between the two images. Once the coefficients have been obtained for each image pair, they are used to approximate the relative rotations and scales of the images. Once the approximate relative shifts, scales, and rotations of the images have been determined, the target coordinates can be approximated. Finally, if there are any images that were left out of the initial image set, they can be added to the solution using an algorithm based on (Kyle, 2004). This initial approximation step is explained in greater detail in (Blonquist and Pack, 2009b).

Step 2: Orthogonal Bundle Adjustment. The next step is to refine the approximations from the first step. This is done using an implementation of the bundle adjustment that follows the form of the standard bundle adjustment, but is based on the orthogonal projection equations (1) rather than the perspective projection equations (3). Specifically, there are six unknowns for each image $(q_x, q_y, q_z, q_w, \Delta x, \Delta y)$ and three unknowns for each point (X, Y, Z). This results in an improved approximation for the image orientations and the target coordinates. This step is explained in greater detail in (Blonquist and Pack, 2009a).

Step 3: Perspective Correction. The first two steps assumed that the image coordinates followed an orthogonal projection. The next step is to correct the original image coordinates (point correspondences) for perspective so that they more closely follow an orthogonal projection. This can be done using equation (9) and requires the approximate image orientations and point coordinates from the previous step. The approximate orthogonal projection scale is used as $\bar{s}$, the approximate IOP are used for (f, x_a, y_a), and the approximate image orientations and target coordinates are used to compute $\lambda(\mathbf{X})$ for each point.

Step 4: Orthogonal Bundle Adjustment. The orthogonal bundle adjustment as explained in step 2 is carried out again using the perspective-corrected coordinates rather than the original image coordinates. This leads to an improved approximation of the image orientations and target coordinates.

Step 5: Conversion to Perspective Projection. The orthogonal solution from the previous step is converted into an approximate perspective solution. The perspective center is approximated using equation (10), and the rotation is approximated as the rotation from the orthogonal solution. Once approximate perspective image orientations are computed, the approximate target coordinates can be updated using the original image coordinates and the perspective projection equations.

Step 6: Perspective Bundle Adjustment. The final step is to perform the well-known standard bundle adjustment based on the perspective projection equations, using the data from the previous step and the original image coordinates.

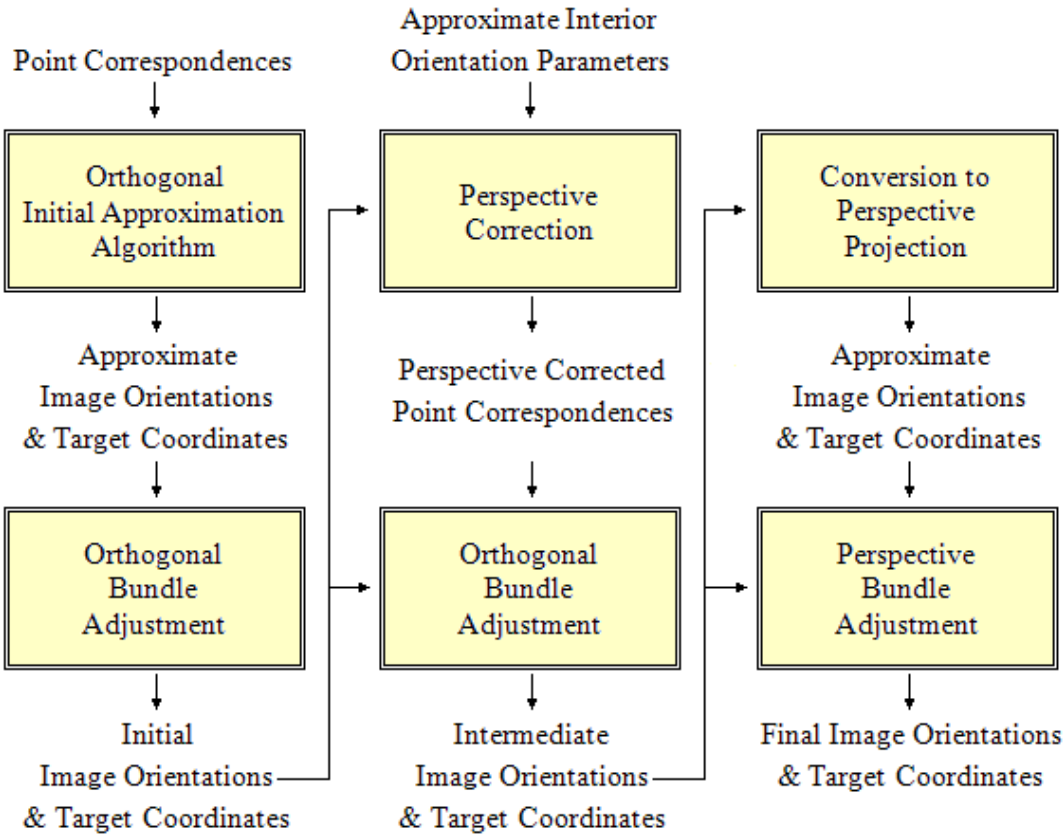

Figure 1. Flow chart of the new algorithm.

EXPERIMENTS

Several experiments were conducted to investigate the performance of the algorithm under various circumstances. Three sets of actual images were analyzed along with several sets of synthetic images. In addition to the algorithm outlined above, the image sets were also analyzed using standard photogrammetric techniques as a means of comparison. For each image set, the relative orientation of two images was approximated following the procedure described in (Pan, Brooks, and Newsam, 1995) and (Pan, Huynh, and Hamlyn, 1995). Given the approximate relative orientation of two images, the coordinates for all of the points common to those two images were then approximated. Additional images were then added to the solution using the DLT and bundle adjustment.

Image Experiments. Three sets of images were collected in San Diego Harbor, California. Two of the image sets are of the US Coast Guard (USCG) vessel Haddock, and one image set was of the USCG vessel Petrel. The specifications for these image sets are given in Table 1 and one image from each image set is shown in Figure 2.

All three of the image sets have many qualities that are common in surveillance imagery. They were taken from varying ranges and aspects; they are images of a distant object for which there is no *a priori* knowledge; there was no control information for the positions of the cameras relative to the target; and the cameras were uncalibrated. The major differences between the image sets are: 1) the range at which they were taken (Image set 1 is the closest range, while Image set 3 is the longest range), 2) the camera that was used for each set, 3) the number of images in each set, and 4) the target itself (although the Haddock and Petrel are of the same class).

A set of point correspondences was collected on each image set and the IOP of each camera/lens combination were approximated. These inputs were then fed into our new algorithm, and then processed using standard photogrammetric techniques.

Table 1. Characteristics of the image sets.

	Image set 1	Image set 2	Image set 3
Target:	Haddock	Haddock	Petrel
# of images:	8	6	4
Camera:	CANON EOS 5D	CANON EOS 20D	CANON EOS 1Ds
Resolution:	12.7 megapixel	8.2 megapixel	16.7 megapixel
Lens:	400 mm	400 mm	560 mm
Approximate range:	300 – 400 m	1100 – 1700 m	2100 – 3000 m
Approximate subtended angle of object:	3.0° - 4.0°	1.0° - 1.5°	0.5°

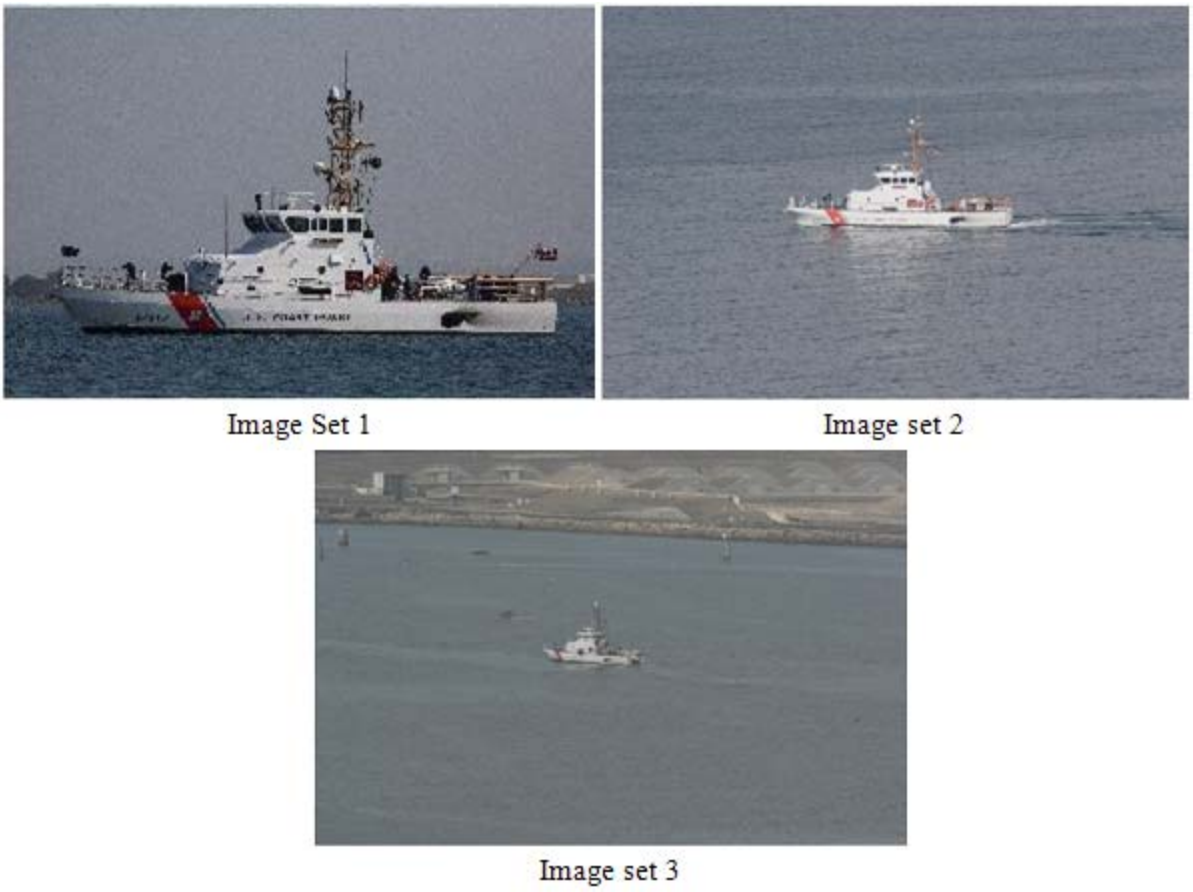

Figure 2. One image from each of the image sets.

For each of the three image sets, the new algorithm converged to a solution successfully. In contrast, the standard photogrammetric method encountered some instability in the second image set, particularly during the relative orientation of two images and during the DLT step. Despite the instability, by trying various image pairs and by changing the order in which the images were added using the DLT, a solution was eventually obtained. The third image set also caused problems for the standard method, but despite trying all possible image combinations, a viable solution was never achieved. The results for the experiments are given in Tables 2 and 3. The results from the new algorithm consist of three solutions: an initial solution at the end of the orthogonal projection step (step 2), an intermediate solution at the end of the perspective-corrected orthogonal projection step (step 4), and the final

solution by perspective projection (labeled as perspective with orthogonal initialization). The standard method consisted of one solution (labeled as perspective projection with standard initialization). Note also that the model has only an approximate scale, so the units of the model are approximate meters, labeled as "~m".

It is worth noting that for Image set 1, the results obtained by the perspective projection are more accurate than the results obtained by either the orthogonal projection, or the perspective-corrected orthogonal projection. This suggests that at this relatively wide subtended angle, the orthogonal projection, though not providing a very accurate result on its own, does provide an adequate starting point from which the perspective projection algorithm can converge to a solution. It is also of note that the perspective projection initialized by the orthogonal projection achieved an almost identical result to the perspective projection initialized by the standard method.

Table 2. Residuals for the three image sets.

	Image set 1	**Image set 2**	**Image set 3**
Average range:	357	1467	2467
# of points:	65	46	46
Mean total residual (pixel)			
Orthogonal Projection:	9.45	1.28	0.67
Perspective-Corrected Orthogonal Projection:	0.88	1.10	0.62
Perspective Projection (w/ orthogonal initialization):	0.88	1.12	0.62
Perspective Projection (w/ standard initialization):	0.88	1.12	error
Maximum total residual (pixel)			
Orthogonal Projection:	56.40	4.11	3.80
Perspective-Corrected Orthogonal Projection:	3.40	3.37	3.81
Perspective Projection (w/ orthogonal initialization):	3.39	3.39	3.57
Perspective Projection (w/ standard initialization):	3.39	3.38	error

Table 3. 1-sigma errors for the three image sets.

	Image set 1	**Image set 2**	**Image set 3**
Average range:	357	1467	2467
# of points:	65	46	46
Mean total 1-sigma error (~m)			
Orthogonal Projection:	0.062	0.033	0.034
Perspective-Corrected Orthogonal Projection:	0.006	0.030	0.031
Perspective Projection (w/ orthogonal initialization):	0.006	0.031	0.031
Perspective Projection (w/ standard initialization):	0.006	0.031	error
Maximum total 1-sigma error (~m)			
Orthogonal Projection:	0.202	0.063	0.110
Perspective-Corrected Orthogonal Projection:	0.016	0.059	0.111
Perspective Projection (w/ orthogonal initialization):	0.015	0.057	0.114
Perspective Projection (w/ standard initialization):	0.015	0.057	error

For Image set 2, the initial solution obtained by the orthogonal projection is still less accurate than the final solution from the perspective projection. But the intermediate solution from the perspective-corrected orthogonal projection essentially matched the precision of the perspective projection. Once again, both perspective projection

solutions are roughly equivalent, despite being initialized in different ways. However, the orthogonal initialization did not encounter any of the instability that burdened the standard method. At this subtended angle it appears that the similarity between the orthogonal projection and perspective projection is high, though there is still a detectable difference.

For Image set 3, the three projections (orthogonal, perspective-corrected orthogonal, and perspective) converged to nearly the same result, indicating that at this narrow subtended angle the difference between the two projections is essentially immeasurable. For this image set, the standard method did not produce a reliable solution. The 1-sigma errors for this image set are virtually identical to those of Image set 2. Higher error associated with the increased range to target is offset by the lower residual errors. Apparently, higher image resolution and the ability to select strong conjugate points for this image set made a significant improvement to the error magnitude.

These tests demonstrate the robustness of the proposed method over three distinct ranges. The method was able to achieve accuracy equal to that obtained through the standard method, and was able to reach a solution in a case where the standard method failed.

Synthetic Image Experiments. A series of tests using synthetic images was also conducted to test the algorithm over a wider range of conditions. A set of 56 synthetic target coordinates were created that roughly mimic the size and shape of the Haddock and Petrel (30.6 x 6.0 x 10.4 ~m). In each test, a base range was chosen and eight image orientations were selected around the target at or near the base range. Three sets of IOP were also created to approximate the three camera/lens combinations used in the real image tests. Each of the eight image orientations was paired with one of the cameras, and a set of synthetic image coordinates were generated with the collinearity equations (3). The raw image coordinates were then perturbed with random noise (magnitude 1.25 pixel), and some image coordinates were deleted to simulate points that are not visible in some images due to occlusion. The image coordinates and approximate IOPs were then fed into our new algorithm and then into the standard photogrammetric algorithms.

For each projection, the resulting model was compared with the initial coordinates using a 3D similarity transform (scale, shift, and rotation). The mean error between the actual coordinates and calculated coordinates was also computed for each test. Figures 3 and 4 show the average actual error in meters plotted versus distance. The zero values plotted on Figure 4 for the standard method indicate a test that failed to converge. Figures 5 and 6 show the average residuals in pixels plotted versus distance. When considering Figures 3 – 6, note that there are a few somewhat distinctive distance intervals that exhibit unique behavior.

Below about 500 meters, the orthogonal projection is quite inaccurate (Figure 3), but is still suitable to initialize a more accurate solution; the perspective-corrected orthogonal projection is not quite able to match the precision of the perspective projection, but is a considerable improvement over the orthogonal projection; and the perspective projection as initialized by the orthogonal solution matches the perspective projection as initialized by the standard method (Figure 4). At this distance interval the residuals for the orthogonal projection (Figure 5) are well above the level of noise (1.25 pixel) that was added to the images; the residuals for the perspective-corrected orthogonal projection begin to deviate above the added noise as well, while the residuals for the perspective projection (Figure 6) remain near the level of noise. At the closest ranges even the perspective results deviate upward slightly due to the fact that approximate IOP were used and not treated as unknowns. In this range the standard method exhibits no instability.

In the distance interval of 500 to 1000 meters, the orthogonal projection is still inaccurate, but continues to converge toward the perspective projection results. The perspective-corrected orthogonal projection is nearly equivalent to the perspective projection. The perspective projection results as initialized by both methods are still nearly the same. Although in some of the tests, the standard method did produce a slightly higher residual.

From about 1000 to 2500 meters, the orthogonal projection gradually improves until it in effect matches the accuracy of the perspective projection. The perspective-corrected orthogonal projection and perspective projection maintain a high level of accuracy. However, the standard method begins to show signs of instability, and eventually becomes quite unstable.

Beyond 2500 meters, the standard method failed for every test, and the three solutions from the new algorithm are nearly equivalent. In none of these cases did the new method fail.

It is also worth noting the difference between the actual error and the 1-sigma error estimates as shown in Figure 7. Below about 1500 meters, the perspective projection is well within 0.01 meters for almost all of the tests. This indicates that at close range the perspective projection is able to predict the error well. Beyond 1500 meters, the perspective predictions begin to deviate somewhat, but remain for the most part within 0.01 meters. Below about 500 meters, the perspective-corrected orthogonal projection quite often under-predicts the actual error, and below about 1500 meters the orthogonal projection under-predicts the error. This is because at these ranges, these models deviate significantly from the true imaging geometry and as such have uncharacterized errors.

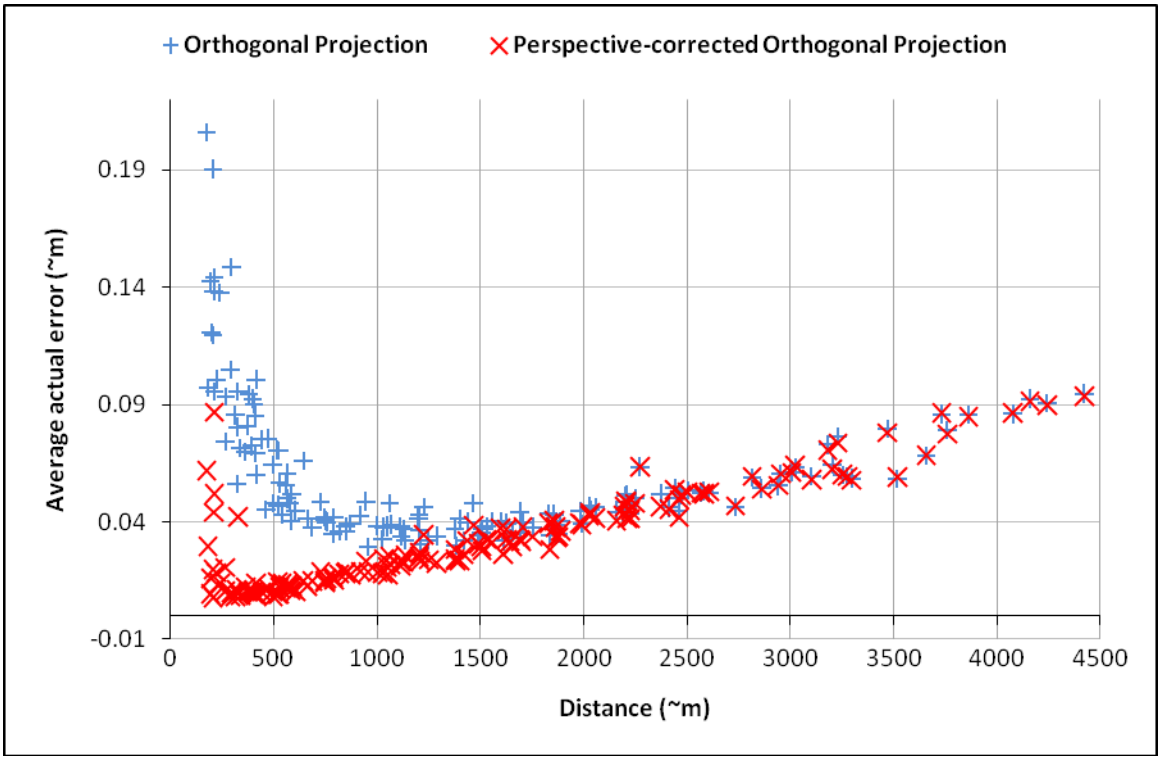

Figure 3. Average actual error for the orthogonal and perspective-corrected orthogonal projections.

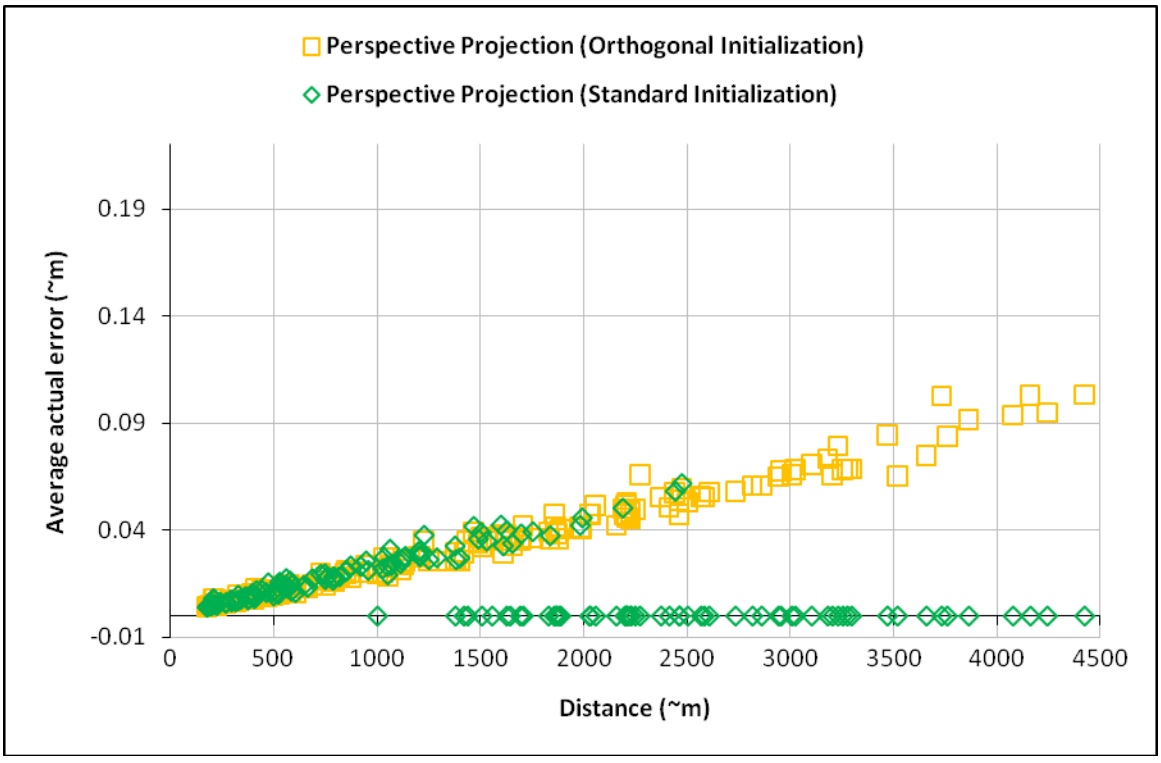

Figure 4. Average actual error for the perspective projection with both initialization methods.

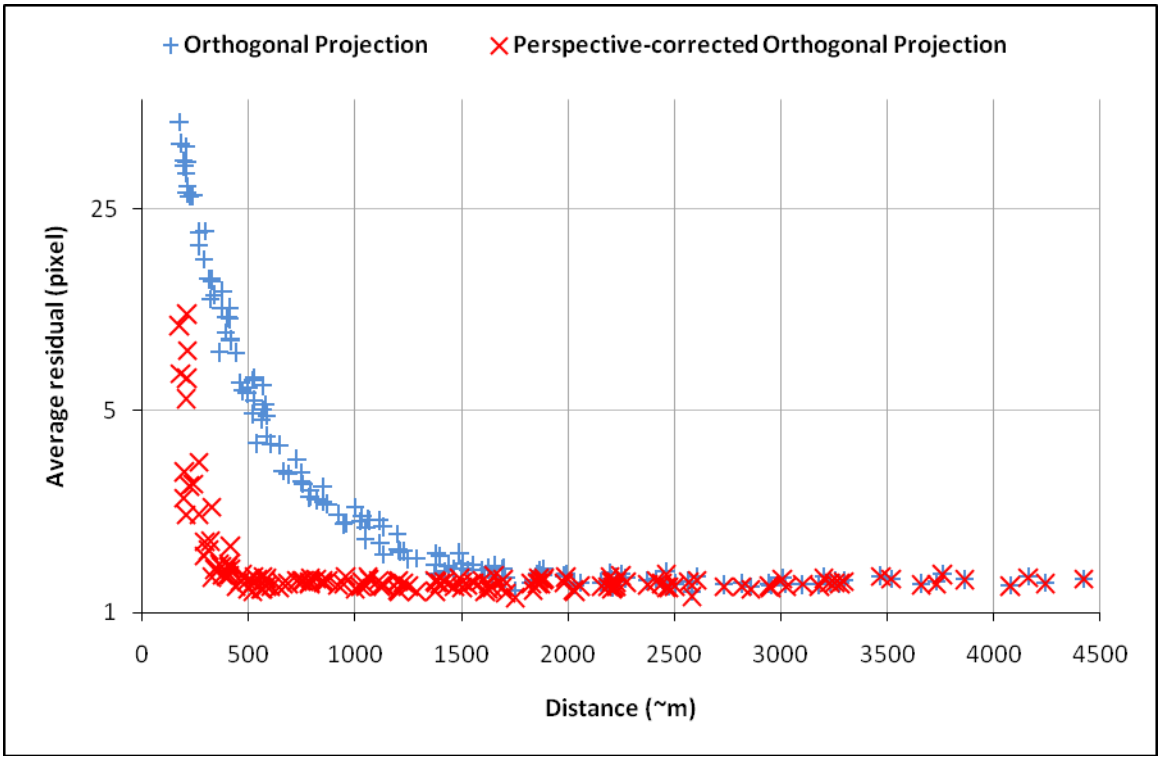

Figure 5. Average residual for the orthogonal and perspective-corrected orthogonal projections.

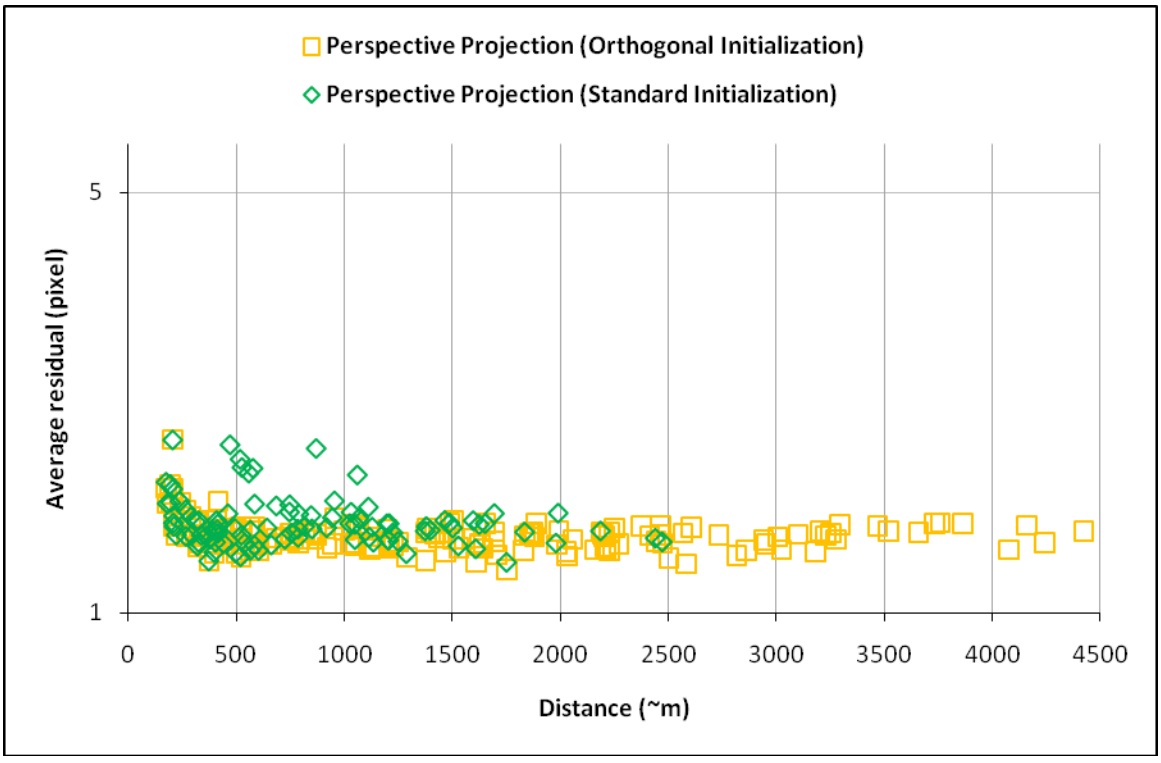

Figure 6. Average residuals for the perspective projections with both initialization methods.

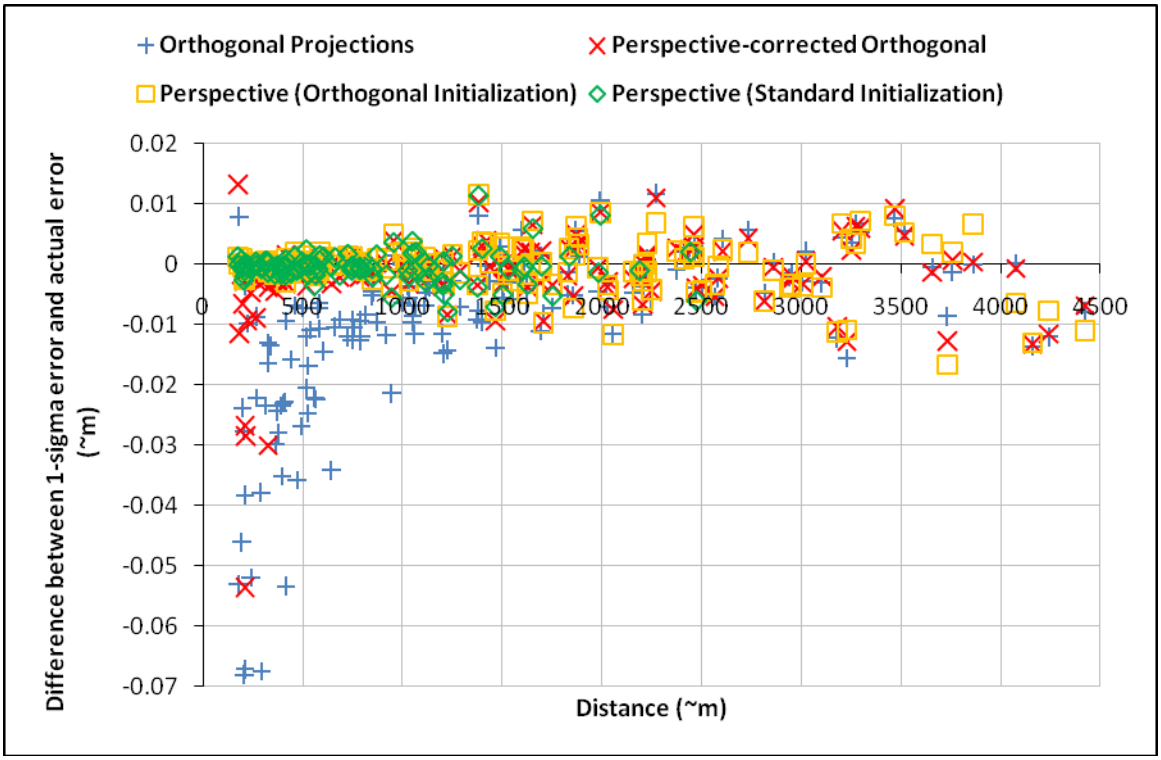

Figure 7. Difference between the actual error and 1-sigma error.

SUMMARY

We have derived a method that solves for the 3D geometry of a target object from a series of images captured from a distance using uncalibrated hand-held cameras. The algorithm requires only a set of point correspondences across three or more images, and the approximate IOP of the cameras. The algorithm has been tested using several sets of images, both real and synthetic, and has been shown to perform well over a wide range of imaging distances, including many cases where standard photogrammetric methods fail.

ACKNOWLEDGMENTS

This research was funded by the Naval Air Warfare Center (NAVAIR) via the STTR/SBIR program with the help of Robert Hintz, NAVAIR China Lake, California. The authors would like to particularly thank T. Dean Cook (NAVAIR) and F. Brent Pack (Lidar Pacific) for their technical contributions and guidance as well as a thorough manuscript review.

REFERENCES

Blonquist, K.F., and R.T. Pack, 2009a. Bundle adjustment for the orthogonal projection with inner constraints, White Paper, Lidar Pacific Corporation, Logan, UT-USA.

Blonquist, K.F., and R.T. Pack, 2009b. Orthogonal photogrammetric solutions without a-priori camera and target Knowledge, White Paper, Lidar Pacific Corporation, Logan, UT-USA.

Huang, T.S., and C.H. Lee, 1989. Motion and structure from orthographic projections, *IEEE Transactions on Pattern Analysis and Machine Intelligence*, 11(5):536-540.

Kyle, S., 2004. Using parallel projection mathematics to orient an object relative to a single image, *The*

Photogrammetric Record, 19(105):38-50.

Ono, T., and S. Hattori, 2002. Fundamental principles of image orientation using orthogonal projection model, *International Archives of Photogrammetry, Remote Sensing and Spatial Information Sciences*, 34(3B):194-199.

Pan, H.P., M.J. Brooks, and G.N. Newsam, 1995. Image resituation: Initial theory, in *Proceedings of SPIE: Videometrics IV*, 2598, 162-173.

Pan, H.P., D.Q. Huynh, and G.K. Hamlyn, 1995. Two-image resituation: Practical algorithm, in *Proceedings of SPIE: Videometrics IV*, 2598, 174-190.